Electric and magnetic dipole transitions from broad *s*-wave neutron resonance in even-even *sd*-shell nuclei

H. Kitazawa, M. Igashira, M. Shimizu, K. Muto, T. Oda, Y. Achiha, Y.-H. Lee, and N. Mukai
Tokyo Institute of Technology, 2-12-1 O-okayama, Meguro-ku, Tokyo 152, Japan
(Received 7 July 1992)

Observations have been performed for electromagnetic transitions from the broad *s*-wave neutron resonances at 658 keV in ^{24}Mg, at 180 keV in ^{28}Si, and at 103 keV in ^{32}S. Capture gamma rays were measured with an anti-Compton NaI(Tl) detector, using a neutron time-of-flight technique. $E1$ and $M1$ transitions from those resonances to low-lying states with a strong single-particle character were found. The deduced partial radiative widths for $E1$ transition are in excellent agreement with the Lane-Mughabghab valence-capture model calculations taking the neutron effective charge, $-Ze/A$. Moreover, it is shown that essential features of the observed $E1$ and $M1$ transitions can be well explained by assuming a configuration-mixing wave function, $\Psi_i(\frac{1}{2}^+)=a(0^+\otimes\frac{1}{2}^+)+b(1^+\otimes\frac{1}{2}^+)+c(1^+\otimes\frac{3}{2}^+)$, for each resonance. The $M1$ transition strengths are compared also with more detailed shell model calculations in the model space of full $(sd)^n$ configurations, using the Wildenthal effective interaction.

PACS number(s): 25.40.Lw, 23.20.Lv, 27.30.+t

I. INTRODUCTION

A lot of experimental data on radiative widths of neutron resonance levels have been reported. However, radiative widths of broad *s*-wave resonances were frequently found to include systematic error [1]. This problem is, in particular, serious for the data measured with neutron-sensitive total energy detectors in time-of-flight experiments. In the experiments, it is intrinsically difficult to distinguish between capture gamma-ray events and the background due to the neutrons strongly scattered in a capture sample. Therefore, a detailed discussion was scarcely given on the structure of broad *s*-wave resonances and on the neutron resonance-capture mechanism.

In the neutron capture on broad *s*-wave resonances in *sd*-shell nuclei, furthermore, strong $M1$ transitions from those resonances to low-lying states with positive parity are predicted, as mentioned below. It seems to be in marked contrast with primary electromagnetic transitions from broad *p*-wave resonance capture, in which primary $M1$ transitions are greatly suppressed [2–4].

So far, it is well known that the $M1$ strength observed with neutron resonance-capture reactions reaches a peak in the vicinity of closed-shell nuclei [5]. For double magic nuclei, the strong $M1$ strength was ascribed to the excitation of collective isovector $M1$ states, which is aroused by coherent nucleon transitions between the filled and empty members of spin-orbit partners [6]. In this physical picture, the $l\cdot s$ particle-hole pairs in the *sd*-shell, $1d_{5/2}$-$1d_{3/2}$, are expected to produce $M1$ states a few MeV above the $l\cdot s$ splitting energy ($\sim$7.0 MeV), on account of a repulsive nature of the spin-dependent particle-hole interaction. Consequently, in electromagnetic transitions from broad *s*-wave resonances in *sd*-shell nuclei, $M1$ transitions would be enhanced by coupling between the *s*-wave neutron single-particle state and those collective $M1$ states.

From such a viewpoint, the present study was devoted to investigating electromagnetic transitions from the broad *s*-wave resonances at 658 keV in ^{24}Mg, at 180 keV in ^{28}Si, and at 103 keV in ^{32}S.

II. EXPERIMENTS

Using a neutron time-of-flight (TOF) technique we have measured gamma-ray spectra from neutron capture on the *s*-wave resonances at 658 keV in ^{24}Mg, at 180 keV in ^{28}Si, and at 103 keV in ^{32}S. Figure 1 shows the experimental arrangement.

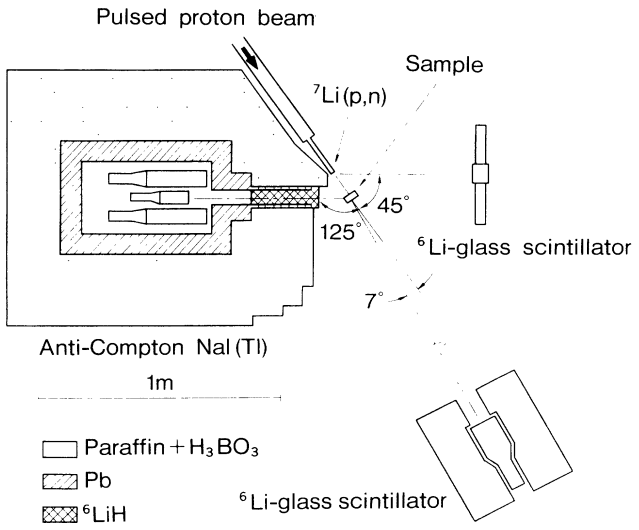

FIG. 1. Experimental arrangement.

Pulsed neutrons were produced from the $^{7}Li(p,n)^{7}Be$ reaction by bombarding a Li-evaporated copper disk with the 1.5-ns bunched proton beam from the 3.2-MV Pelletron Accelerator of the Research Laboratory for Nuclear Reactors in the Tokyo Institute of Technology. The typical proton beam current was 10 μA at 2-MHz pulse repetition rate. The neutron source target was cooled by spraying water on the target from outside to prevent lithium from being scattered and lost. Capture samples were disks of natural magnesium, silicon, and sulfur, which were placed 156 mm away from the neutron source at right angles to the proton-beam direction. The sample thickness was determined so as to give a neutron transmission of about 70% at each resonance peak, in order to diminish the correction factor for neutron multiple scattering and self-shielding described in Sec. III B.

Capture gamma rays were detected with a 76-mm diameter by 152-mm NaI(Tl) detector, which was centered in a 254-mm diameter by 280-mm NaI(Tl) hollow anti-Compton detector surrounded by a heavy shield [7]. The gamma-ray detector was located at a distance of 80 cm from the sample, with its axis at an angle of 125° to the proton-beam direction.

In the present experiments a special consideration was also given to observing capture gamma rays from strong s-wave resonances. The 500-g ^{6}LiH powder (95% enriched lithium-6), which was packed in a 63-mm diameter by 300-mm metallic aluminum case lined with acrylic resin to protect against corrosion, was inserted into the collimator of the gamma-ray detector, in order to remove the neutrons strongly scattered into the detector by the sample [8].

Figure 2 shows the background gamma-ray pulse-height spectrum in the experiments, in comparison to the spectrum without ^{6}LiH. In the figure, the peak (a) is ascribed to gamma rays from the thermal neutron capture by iodine in the NaI(Tl) detector. The neutron capture gamma rays originally exhibit a soft spectrum. However, since those reactions are generated in the interior of the detector, cascade gamma rays are almost detected with high possibility, and therefore the peak appears at the neutron binding energy (6.8 MeV) of ^{127}I. Part (b) in the spectrum was produced by β decays of the ^{128}I nucleus ($t_{1/2}=25$ min). It is found that the ^{6}LiH powder diminishes the neutrons scattered into the detector, and consequently brings an extreme decrease of the background produced by the $^{127}I(n,\gamma)^{128}I$ reaction. Since the neutrons scattered by the sample into the collimator arouse 70–80% of the gamma-ray background, ^{6}LiH is very efficient to increase the signal to background (S/N) ratio.

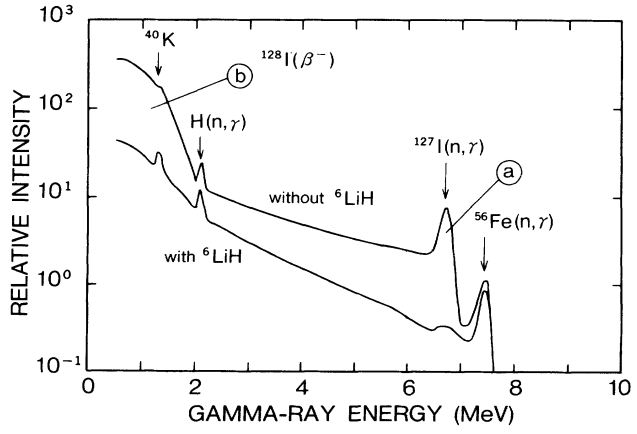

FIG. 2. Background gamma-ray pulse-height spectra.

However, a gamma-ray peak at 7.6 MeV, which is due to the thermal neutron capture by the ^{56}Fe nucleus included in the structural material of the heavy shield, and a gamma-ray peak at 2.2 MeV, which is due to the thermal neutron capture by hydrogen included in the neutron shielding material, are hardly depressed even in the use of ^{6}LiH. While, the gamma-ray detection efficiencies at 2.0 and 6.0 MeV decrease by 50% and 30%, respectively, because of the gamma-ray absorption in the ^{6}LiH and aluminum case.

The response matrix of the gamma-ray detector, which includes information on the detection efficiency and the gamma-ray shielding effects of ^{6}LiH, was determined with the aid of gamma rays from calibrated radioactive sources, an Am-Be neutron source, and the $^{19}F(p,\alpha\gamma)^{16}O$ and $^{27}Al(p,\gamma)^{28}Si$ reactions [9].

Incident neutron spectra were measured by means of a TOF method without the sample, employing a 102-mm diameter by 6.4-mm ^{6}Li-glass scintillation detector. The detector was placed at an angle of 7° to the photon-beam direction, 1–5 m away from the neutron source. The measurement at this angle gave approximately an averaged incident neutron spectrum on the sample. Figure 3 shows the neutron flux distributions used for the experiments on magnesium, silicon, and sulfur. Those spectra were normalized to one neutron. However, the spectra for the 180-keV resonance experiment on ^{28}Si and for the 103-keV resonance experiment on ^{32}S were obtained by normalizing the neutron energy spectrum within a TOF gate width, because monoenergetic neutrons were unavailable at those resonance energies. In the 658-keV resonance experiment on ^{24}Mg, we took measurements for three kinds of neutron-flux distributions, (A), (B), and (C), with different average energies, in order to separate a contribution of the 642-keV $p_{1/2}$-wave narrow resonance overlapping with the 658-keV resonance. Those resonance parameters [10,11] are given in Table I.

Capture events detected by the gamma-ray detector were stored in a minicomputer as two-dimensional data on TOF and pulse height. Figure 4 shows the TOF spectra measured for magnesium, silicon, and sulfur samples.

TABLE I. Resonance parameters Refs. [10,11].

	E_R(keV)	J^π	Γ_n(keV)	$g\Gamma_n\Gamma_\gamma/\Gamma$ (eV)
^{24}Mg	641.9±0.6	$\frac{1}{2}^-$	0.9±0.2	1.2±0.2
	658.5±0.7	$\frac{1}{2}^+$	21±2	7.7±0.9
^{28}Si	180.0[a]	$\frac{1}{2}^+$	31[a]	5.6±2.2
^{32}S	102.71±0.03	$\frac{1}{2}^+$	15.0±0.1	7.79±0.17

[a]Reference [11].

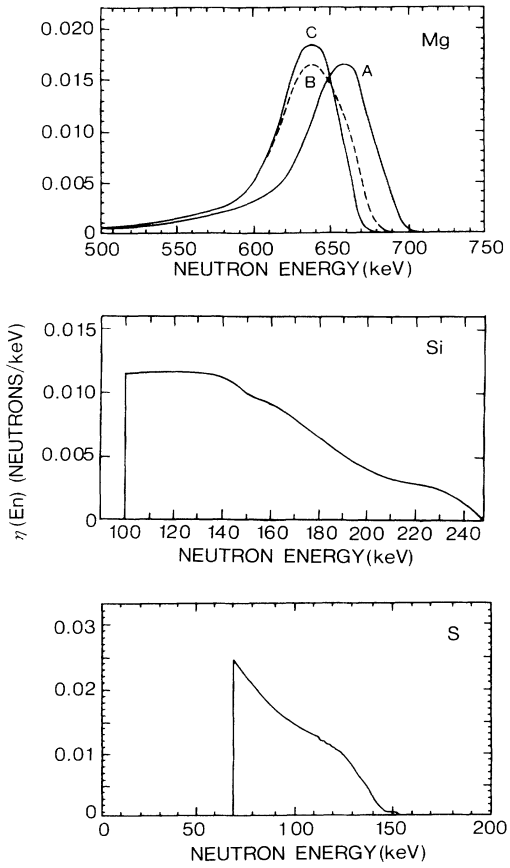

FIG. 3. Neutron flux energy distributions normalized to one neutron used for the experiments on magnesium, silicon, and sulfur.

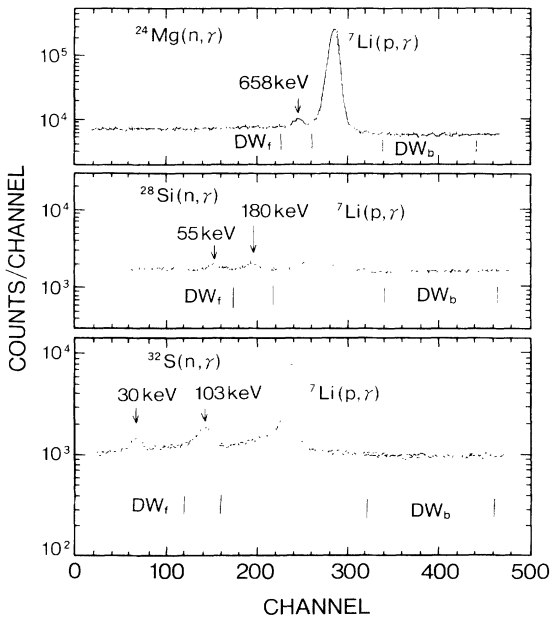

FIG. 4. Time-of-flight spectra measured with magnesium, silicon, and sulfur samples.

The overall time resolution was 3.8 ns (FWHM) for gamma rays above 0.5 MeV. In order to illustrate the S/N ratio, as an example, we show in Fig. 5(a) the normalized foreground and background gamma-ray pulse-height spectra obtained from the 180-keV resonance experiment on ^{28}Si. The foreground spectrum was measured by setting a suitable gate (DW$_f$) at the position of the capture gamma-ray peak in the TOF spectrum. The background spectrum was taken as being time independent, and measured similarly by setting a gate (DW$_b$) about three times wider than the foreground gate (DW$_f$). The net gamma-ray pulse height spectrum in Fig. 5(b) was obtained by subtracting the background from the foreground.

The capture cross sections of ^{24}Mg, ^{28}Si, and ^{32}S were determined by normalizing the capture gamma-ray yield of each nucleus to that of ^{197}Au. The yield of ^{197}Au was related to the ENDF/B-V neutron capture cross section [12] of ^{197}Au by means of a pulse-height weighting technique [13]. Therefore, measurements were performed alternately between the sample and gold runs. Both data were normalized by neutron counts of another ^{6}Li-glass scintillation detector installed at an angle of 45° to the

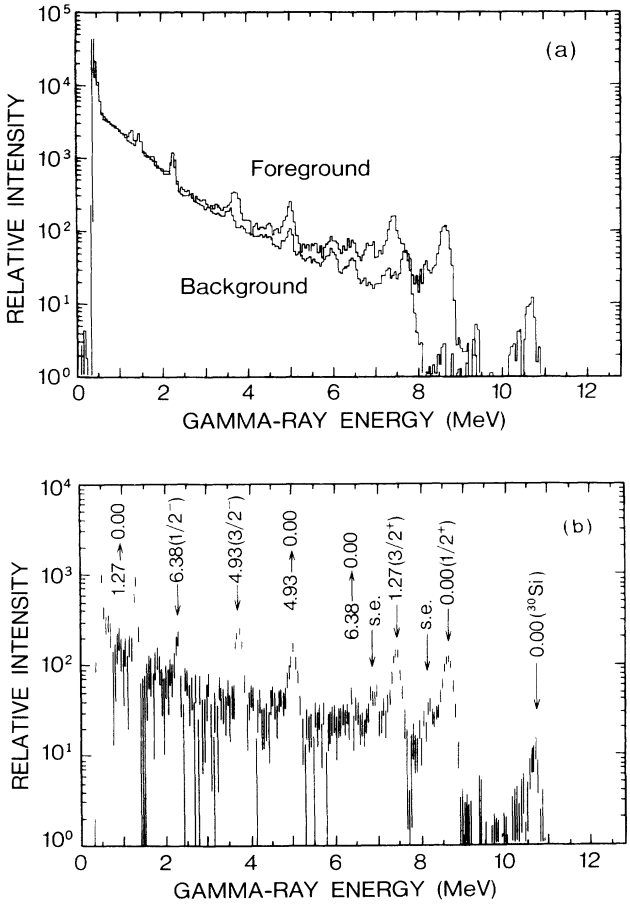

FIG. 5. (a) Foreground and background gamma-ray pulse-height spectra in the 180-keV resonance experiment on ^{28}Si. (b) Net capture gamma-ray pulse-height spectrum in the 180-keV resonance experiment on ^{28}Si.

proton-beam direction so as to view directly the neutron source.

III. EXPERIMENTAL RESULTS

A. Resonance capture gamma-ray spectra

Figures 6, 7, and 8 show the capture gamma-ray spectra. Those spectra were obtained from unfolding the net gamma-ray pulse-height spectra in Sec. II, using the computer program FERDOR [14] and the matrix represented by a product of the gamma-ray response matrix and a correction matrix. The correction matrix was generated by a Monte Carlo method to take into account the photoelectric absorption, Compton scattering, and pair creation of capture gamma rays in the sample. For reference we show the gamma-ray attenuation factors C_γ of the sample in Table II, which are diagonal elements of the correction matrix. The correction was found to be 10% at most.

1. 180-keV resonance in ^{28}Si

As shown in Fig. 6, primary gamma rays have been observed for the $M1$ transitions to the ground ($\frac{1}{2}^+$) and 1273-keV ($\frac{3}{2}^+$) states in ^{29}Si and for the $E1$ transition to the 4934-keV ($\frac{3}{2}^-$) state. Those transitions are to the states with a large spectroscopic factor. The 1273-keV ($\frac{3}{2}^+$) state transition is also conceivable to be of electric quadrupole. However, such a strong primary $E2$ transition has never been observed in neutron resonance-capture reactions. Furthermore, a core-particle coupling model calculation [15] shows that the collective $E2$ transitions, $[(0^+\otimes s_{1/2})\rightarrow(2^+\otimes s_{1/2})]$ and $[(2^+\otimes d_{3/2})\rightarrow(0^+\otimes d_{3/2})]$, account for only 9 meV of the radiative width; the observed $E2$ transition strength [16] between the ground state (0^+) and first excited state (2^+) in ^{28}Si was taken as the $E2$ core transition strength. Therefore, it is most probable that the 1273-keV state transition is assumed to be of magnetic dipole. Here, in particular we note that the primary $M1$ transitions to the ground ($\frac{1}{2}^+$) and 1273-keV ($\frac{3}{2}^+$) states are barely observed in the thermal neutron capture [17]. The remarkable difference between resonance and thermal neutron capture may characterize the reaction mechanism of each process.

A gamma-ray peak at 4.9 MeV is due to the cascade transition from the 4934-keV ($\frac{3}{2}^-$) state to the ground

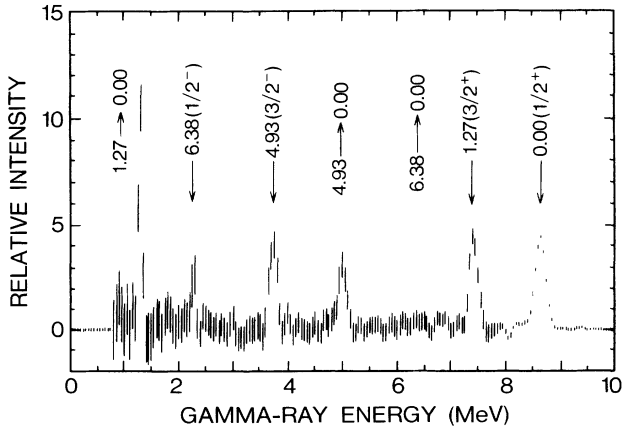

FIG. 6. Capture gamma-ray energy spectrum in the 180-keV resonance experiment on ^{28}Si.

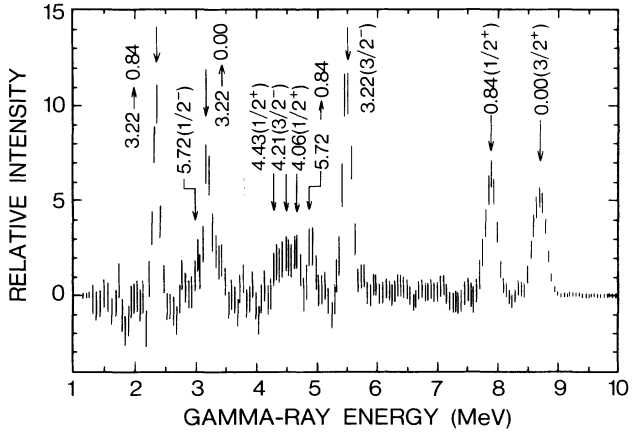

FIG. 7. Capture gamma-ray energy spectrum in the 103-keV resonance experiment on ^{32}S.

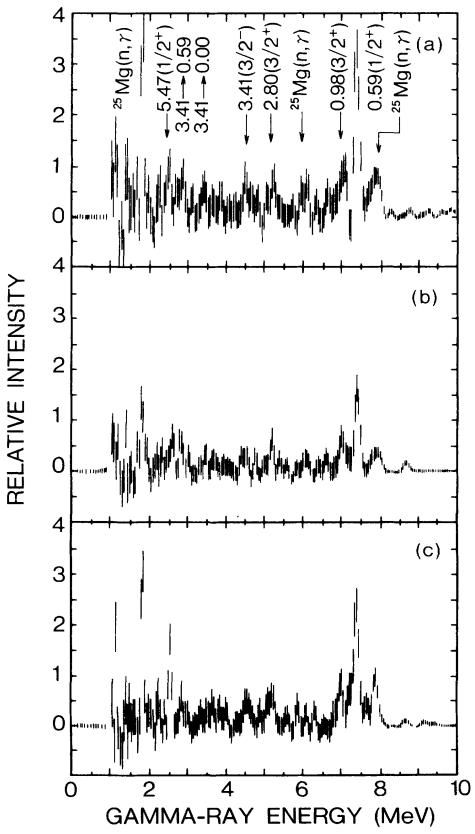

FIG. 8. Capture gamma-ray energy spectra in the 658-keV resonance experiment on ^{24}Mg obtained (a) for the neutron flux A, (b) for the neutron flux B, and (c) for the neutron flux C.

TABLE II. Correction factors for neutron multiple scattering (C_{nm}), for neutron self-shielding (C_{ns}), and for gamma-ray attenuation (C_γ) in the sample.

	Resonance energy (keV)	C_{nm}	C_{ns}	C_γ
^{24}Mg	658	1.13	0.87	0.90–0.95
	642	1.13	0.88	0.90–0.95
^{28}Si	180	1.28	0.88	0.90–0.96
^{32}S	103	1.66	0.74	0.90–0.95

state. The observed strength ratio of the cascade transition to the primary 4934-keV state transition is 0.86±0.32, which is in substantial agreement with the branching ratio, 0.94±0.01 [18], for the cascade transition. Also, a gamma-ray peak at 2.3 MeV may be due to the primary transition to the 6381-keV ($\frac{1}{2}^-$) state. However, this peak seems to include a large contribution of the transition from the 2236-keV (2^+) state to the ground (0^+) state in ^{30}Si, produced by neutron capture on ^{29}Si. The reason is that the primary gamma rays to the ground state in ^{30}Si are found at 10.7 MeV, and that a gamma-ray peak at 6.4 MeV is imperceptible, in spite of the large branching ratio, 0.63±0.13 [18], for the transition from the 6381-keV state to the ground state [see Fig. 5(b)].

2. 103-keV resonance in ^{32}S

The primary $M1$ transitions to the ground ($\frac{3}{2}^+$) and 840-keV ($\frac{1}{2}^+$) states and the primary $E1$ transition to the 3220-keV ($\frac{3}{2}^-$) state have been identified, as shown in Fig. 7. Those transitions are of strong single-particle character. As in the case of ^{28}Si, the primary transitions to the $\frac{1}{2}^+$ and $\frac{3}{2}^+$ states, which are extremely weak in the thermal neutron capture [19], are enhanced.

The gamma-ray peaks at 3.2 and 2.4 MeV may be due to the cascade transitions from the 3220-keV state to the ground and 840-keV states, respectively. The observed strength ratio of the cascade transition [3220 keV→840 keV] to the primary 3220-keV state transition is 0.69±0.07, which is in good agreement with the branching ratio, 0.64±0.02 [19], for the cascade transition. However, the strength ratio of the cascade transition [3220 keV→0 keV] to the primary 3220-keV state transition is 0.78±0.09, which is much larger than the branching ratio, 0.35±0.02 [19], for the cascade transition. Probably, this is because the gamma-ray peak at 3.2 MeV includes the primary transition to the 5715-keV ($\frac{1}{2}^-$) state with a strong single-particle character and the cascade transition, [4210 keV→840 keV], with the large branching ratio, 0.93±0.04 [19]. It is also supposed from spreading of the bottom of the gamma-ray peak.

A gamma-ray peak at 4.9 MeV is due to the cascade transition [5717 keV→840 keV] with the large branching ratio, 0.76±0.02 [19]. Also, a broad gamma-ray peak around 4.5 MeV may include the primary transitions to the 4055-keV ($\frac{1}{2}^+$), 4210-keV ($\frac{3}{2}^-$), and 4425-keV ($\frac{1}{2}^+$) states.

3. 658-keV resonance in ^{24}Mg

As mentioned in Sec. II, there exists the 642-keV $p_{1/2}$-wave narrow resonance in the vicinity of the 658-keV s-wave resonance in ^{24}Mg. In order to separate the contributions of both resonances, the experiment was performed for three kinds of neutron-flux distributions given in Fig. 3. Figure 8(a) shows a gamma-ray spectrum measured using the neutron flux, (A), with an average neutron energy close to the 658-keV resonance. The gamma-ray spectra in Figs. 8(b) and 8(c) were measured using the neutron fluxs, (B) and (C), with an average neutron energy close to the 642-keV resonance, respectively.

As seen from Fig. 8(a), gamma-ray peaks were obtained for the primary $M1$ transitions to the 585-keV ($\frac{1}{2}^+$), 975-keV ($\frac{3}{2}^+$), and 2801-keV ($\frac{3}{2}^+$) states in ^{25}Mg and for the primary $E1$ transition to the 3414-keV ($\frac{3}{2}^-$) state. Those transitions are to the states with a large spectroscopic factor. A gamma-ray peak at 2.8 MeV is due to the cascade transition [3414 keV→585 keV], with the large branching ratio, 0.76±0.01 [18]. However, the peak may include a small contribution of the cascade transition, [2801 keV→0 keV], because the observed strength ratio of the cascade transition [3414 keV→585 keV] to the primary 3414-keV state transition is 0.94±0.14. Also, a gamma-ray peak at 3.4 MeV is due to the cascade transition [3414 keV→0 keV].

A gamma-ray peak at 2.5 MeV is due to the primary transition to the 5474-keV ($\frac{1}{2}^+$) state. We note that in Fig. 8(c) this peak is in particular enhanced in comparison to the other gamma-ray peaks. Probably, the primary 5474-keV state transition is mainly from the 642-keV resonance.

The gamma-ray peaks at 8.0 and 6.0 MeV, if those gamma rays were produced by the ^{24}Mg$(n,\gamma)^{25}$Mg reaction, would be ascribed to the primary $E2$ transitions to the ground ($\frac{5}{2}^+$) and 1965-keV ($\frac{5}{2}^+$) states. Therefore, both gamma-ray peaks would have been produced by the primary transitions to the 3941-keV (3^+) and 5715-keV (4^+) states in ^{26}Mg. A strong gamma-ray peak at 1.8 MeV due to the transition from the 1809-keV (2^+) state to the ground state (0^+) in ^{26}Mg may also support this statement.

B. Partial radiative widths

The partial capture cross section of a sample averaged with a neutron-flux distribution, $\langle\sigma_{\gamma f}(\mathrm{S})\rangle$, is related to the average total capture cross section of ^{197}Au, $\langle\sigma_\gamma(\mathrm{Au})\rangle$, as follows:

$$\langle\sigma_{\gamma f}(\mathrm{S})\rangle = CR\frac{\phi(\mathrm{Au})}{\phi(\mathrm{S})}\frac{N_{\gamma f}(\mathrm{S})}{Y_\gamma(\mathrm{Au})}\langle\sigma_\gamma(\mathrm{Au})\rangle \tag{1a}$$

with

$$C=\frac{(C_{nm}C_{ns})^{\mathrm{Au}}}{(C_{nm}C_{ns})^{\mathrm{S}}} \tag{1b}$$

and

$$R=\frac{(r^2n)^{\mathrm{Au}}}{(r^2n)^{\mathrm{S}}}\ , \tag{1c}$$

where r and n are the radius and thickness (atoms/b) of the sample, respectively; $N_{\gamma f}(S)$ is the partial capture yield for the transition to the state, f, in a residual nucleus, which was obtained by summing up the counts on a corresponding gamma-ray peak in the unfolded spectrum; $Y_\gamma(\mathrm{Au})$ is the total capture yield of ^{197}Au, which was obtained from the capture gamma-ray spectrum, using a pulse-height weighting technique [13]. The quantity ϕ is the total neutron counts measured at an angle of 45° to the proton-beam direction; C_{nm} is the correction factor for neutron multiple scattering, which was calculated by a Monte Carlo method, taking account of neutron scattering and capture in the sample; C_{ns} is the correction factor for neutron self-shielding in the sample, which was calculated by means of an analytical method. Tables II and III show the correction factors and the thickness of the samples used in experiment, respectively. The average capture cross section $\langle \sigma_\gamma(S) \rangle$ was calculated as

$$\langle \sigma_\gamma(S) \rangle = \int \sigma_\gamma(E)\eta(E)dE \ , \tag{2}$$

where η (E) is the normalized neutron flux distribution given in Fig. 3. The average capture cross section of ^{197}Au was calculated using the evaluated value of the ENDF/B-V data file [12].

Since the interference between resonance and off-resonance capture is neglected to a good approximation, the average partial capture cross section $\langle \sigma_{\gamma f}(S) \rangle$ is connected to the partial radiative width, $\Gamma_{\gamma f}$:

$$\langle \sigma_{\gamma f}(S) \rangle = \alpha g \frac{\Gamma_n \Gamma_{\gamma f}}{\Gamma} + \sigma_{\gamma f}(\mathrm{off}) \tag{3a}$$

with

$$\alpha \equiv \int \pi \lambda\!\!\!^{-2}(E) \frac{\Gamma \eta(E)}{(E-E_R)^2 + (\Gamma/2)^2} dE \ , \tag{3b}$$

where g is a statistical factor and $\lambda\!\!\!^{-}$ (E) is the de Broglie wavelength of an incident neutron with energy E. The resonance parameters E_R, Γ, and Γ_n are the resonance energy, total width, and neutron width, respectively.

The partial off-resonance capture cross sections $\sigma_{\gamma f}$(off) were calculated on the basis of the potential-capture theory [20], using the computer program HIKARI [21]. The calculations include the systematic error of 20–30 %, which results from the ambiguity in a choice of the optical potential parameters used in the calculation. However, those cross sections account for at most 15% of the average partial capture cross sections $\langle \sigma_{\gamma f}(S) \rangle$. Therefore, the error of partial radiative widths due to this ambiguity is only a few percent, and it is not so serious as compared with the statistical error. The error of partial radiative widths was calculated, including the statistical error (10–30 %), the error of the detection efficiency of gamma rays (3–7 %), the error of the total capture yield of gold (5%), and the error of the capture cross section of gold (5%).

TABLE III. Thickness of the capture samples.

Sample thickness (atoms/b)		
Mg	Si	S
6.80×10^{-2}	4.61×10^{-2}	3.63×10^{-2}

Table IV shows the observed partial radiative widths of the 180-keV s-wave resonance in ^{28}Si. Those values are about half of our previous ones [22]. Since a fault in data processing was found for the previous experiment on ^{28}Si, we have remeasured the radiative width. As a result, the sum of the observed partial radiative widths for the ground, 1273-keV, 4934-keV, and 6381-keV state transitions was obtained to be 4.33±0.59 eV, which is in agreement with the evaluated total radiative width, 5.6±2.2 eV, of Mughabghab *et al.* [10], within error. However, as mentioned in Sec. III A 1, the primary transition to the 6381-keV state includes a large contribution of the ^{29}Si$(n,\gamma)^{30}$Si reaction. Therefore, the evaluated value of Mughabghab *et al.* seems to be a little too large.

Table V shows the observed radiative widths of the 103-keV s-wave resonance in ^{32}S. Since the primary transitions to the 4055-keV ($\frac{1}{2}^+$), 4210-keV ($\frac{3}{2}^-$), and 4425-keV ($\frac{1}{2}^+$) states could not be separated, the total width of those transitions is given in the table. The partial radiative width for the 5715-keV ($\frac{1}{2}^-$) state transition was derived from the strength of the cascade transition from the 5715-keV ($\frac{1}{2}^-$) state to the 840-keV ($\frac{1}{2}^+$) state, using the branching ratio, 0.76±0.02, observed by Raman *et al.* [19] in the thermal neutron capture by ^{32}S.

The sum of the observed partial radiative widths is 4.29±0.32 eV, which is about half of the total radiative width, 7.79±0.17 eV, evaluated by Mughabghab *et al.* [10]. In the present experiment, there would be no possibility of missing such a strong primary transition which removes the large discrepancy between both values. Probably, the evaluated value of Mughabghab *et al.* is too large.

As for ^{24}Mg, in order to obtain partial radiative widths of the 658-keV s-wave resonance, Eq. (3a) must be modified to include a contribution of the 642-keV $p_{1/2}$-wave resonance. The total width of the 642-keV resonance is very narrow (<1 keV), and therefore the resonance integral in Eq. (3b) is approximated by

$$\alpha' \approx 2\pi^2 \lambda\!\!\!^{-2}(E'_R)\eta(E'_R) \ . \tag{4}$$

Thus, instead of Eq. (3a) the average capture cross section is expressed by the sum of the contributions of both resonances as

$$\langle \sigma^i_{\gamma f}(S) \rangle = \alpha^i g \frac{\Gamma_n \Gamma_{\gamma f}}{\Gamma} + \alpha^{i'} g' \frac{\Gamma'_n \Gamma'_{\gamma f}}{\Gamma'} + \sigma_{\gamma f}(\mathrm{off}) \ , \tag{5}$$

where the superscript i distinguishes three experiments using the neutron-flux distributions (A), (B), and (C) shown in Fig. 3, and the primed resonance parameters denote those of the 642-keV resonance. From Eq. (5) we have

$$y = g \frac{\Gamma_n \Gamma_{\gamma f}}{\Gamma} x + g' \frac{\Gamma'_n \Gamma'_{\gamma f}}{\Gamma'} \tag{6a}$$

with

TABLE IV. Partial radiative widths of the 180-keV s-wave resonance in ^{28}Si.

E_x (keV)	θ_f^2	Partial radiative widths (eV) Present	Valence	*CM*
$0(\frac{1}{2}^+)$	0.55	1.53±0.31		(1.53)
$1273(\frac{3}{2}^+)$	1.00	1.45±0.33		(1.45)
$4934(\frac{3}{2}^-)$	0.59	0.90±0.33	1.15	(0.90)
$6381(\frac{1}{2}^-)$	0.52	0.45±0.19[a]	0.18	0.18

[a]The value shows the upper limit of the partial radiative width (see text).

$$x \equiv \frac{\alpha^i}{\alpha^{i'}} \tag{6b}$$

and

$$y \equiv \frac{\langle \sigma_{\gamma f}^i(\mathrm{S}) \rangle - \sigma_{\gamma f}(\mathrm{off})}{\alpha^{i'}} . \tag{6c}$$

Three different experiments generate three independent data sets of x and y, and consequently the partial resonance kernels, $g\Gamma_n\Gamma_{\gamma f}/\Gamma$ and $g'\Gamma_n'\Gamma_{\gamma f}'/\Gamma'$, in Eq. (6a).

Using the observed data, we obtained the values of x and y for the transitions to low-lying states in ^{25}Mg, as shown by the solid circles in Fig. 9. The least-square fitting of a straight line to those points generates partial resonance kernels: the gradient of the straight line and its intercept on the y axis represent the partial resonance kernels of the 658- and 642-keV resonances, respectively. The results are given in Table VI. From those resonance kernels, the partial radiative widths of the 658-keV s-wave resonance in ^{24}Mg are derived, as given in Table VII.

The sum of the observed partial resonance kernels of the 658-keV broad resonance is 1.25±0.50 eV, which is much smaller than the evaluated resonance kernel, 7.7±0.9 eV, of Mughabghab *et al.* [10]. However, it is unlikely that some strong transitions to compensate this discrepancy are missed in the present experiment. The sum for the 642-keV narrow resonance is 1.71±0.31 eV, being in substantial agreement with the evaluated resonance kernel, 1.2±0.2 eV, of Mughabghab *et al.* [10]. Moreover, as expected in Sec. III A 3, the 5474-keV $(\frac{1}{2}^+)$ state transition has a dominant kernel for the 642-keV resonance.

IV. MODEL CALCULATIONS AND DISCUSSION

A. Electric dipole transitions

As seen from Tables IV, V, and VII, the primary transitions from the broad s-wave resonances are to the final states with a strong single-particle character. Therefore, the observed radiative widths for $E1$ transition were compared with the calculations using the computer program VALENCE [23], which was programmed on the basis of the valence-capture model of Lane and Mughabghab [24]. The model produces the partial radiative width, $\Gamma_{\gamma f}$, for the $E1$ transition to a final state, f:

$$\Gamma_{\gamma f} = \Gamma_n \frac{16\pi}{9\hbar} k_\gamma^3 \bar{e}^2 \theta_f^2 \left[\frac{1}{\mathrm{Im}\tan\delta(\mathrm{opt})} \mathrm{Im} \int_0^\infty U_f(r) r U_i(r) dr \right]^2$$
$$\times \frac{3}{4\pi}(2J_f+1)(2j_i+1)(2j_f+1)(2l_i+1)[(l_i 010|l_f 0) W(l_i j_i l_f j_f; \tfrac{1}{2}1) W(j_i J_i j_f J_f; I1)]^2 , \tag{7}$$

TABLE V. Partial radiative widths of the 103-keV s-wave resonance in ^{32}S.

E_x (keV)	θ_f^2	Partial radiative widths (eV) Present	Valence	*CM*
$0(\frac{3}{2}^+)$	0.70	0.99±0.15		(0.99)
$840(\frac{1}{2}^+)$	0.40	1.01±0.16		(1.01)
$3220(\frac{3}{2}^-)$	0.48	1.36±0.15	1.40	(1.36)
$4210(\frac{3}{2}^-)$	0.08	0.66±0.15[b]	0.15	0.13
$5715(\frac{1}{2}^-)$	0.55[a]	0.27±0.09	0.22	0.26

[a]Reference [28].
[b]The value shows the upper limit of the partial radiative width (see text).

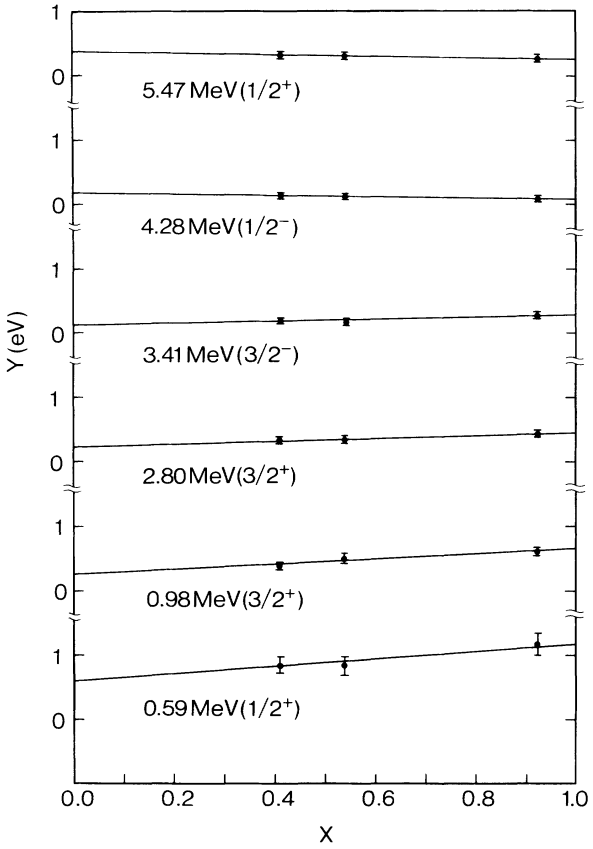

FIG. 9. Plotting for a deduction of the 642- and 658-keV resonance kernels. X and Y are given by Eqs. 6(b) and 6(c), respectively.

where Γ_n is the neutron width, k_γ is the wave number of gamma rays, $\bar{e}$ is the neutron effective charge $(-Ze/A)$, and θ_f^2 is the spectroscopic factor of a final state. The quantity I is the target spin, J is the spin of a residual nucleus, j is the total spin of a neutron single-particle state, and l is the orbital angular momentum. The geometrical factors, Clebsch-Gordon coefficient $(abcd|ef)$ and Racah coefficient $W(abcd;ef)$, are produced by a vector coupling of spin and orbital angular momentum. The subscripts i and f denote the initial (resonance) and final states, respectively. The initial-state wave function $U_i(r)$

TABLE VI. Partial resonance kernels of the 642-keV $p_{1/2}$-wave resonance and the 658-keV s-wave resonance in ^{24}Mg.

	Partial resonance kernels (eV)	
E_x (keV)	642-keV resonance	658-keV resonance
585($\frac{1}{2}^+$)	0.60±0.26	0.59±0.42
975($\frac{3}{2}^+$)	0.19±0.10	0.45±0.15
2564($\frac{1}{2}^+$)		
2801($\frac{3}{2}^+$)	0.23±0.08	0.23±0.13
3414($\frac{3}{2}^-$)	0.13±0.07	0.17±0.11
4277($\frac{1}{2}^-$)	0.18±0.05	−0.08±0.14
5474($\frac{1}{2}^+$)	0.38±0.09	−0.11±0.13

is an optical-model solution, which has the asymptotic form

$$U_i(r) \underset{r\to\infty}{\sim} \frac{1}{v^{1/2}}[\sin(kr-\tfrac{1}{2}l_i\pi) + \tan\delta(\text{opt})\cos(kr-\tfrac{1}{2}l_i\pi)] , \quad (8)$$

where k is the wave number of an incident neutron with velocity, v, and δ(opt) is the optical-model phase shift. Moreover, the real central potential depth in the optical potential was adjusted so that the real part of the initial-state wave function with a $2s_{1/2}$ character resonated in the nuclear internal region:

$$\left.\frac{d\,\mathrm{Re}[U_i(r)]}{dr}\right|_{r=R} = 0 , \quad (9)$$

where R is the nuclear radius. The final-state wave function $U_f(r)$ was obtained using a Woods-Saxon potential searched so as to reproduce the observed neutron binding energy. In the calculation of those wave functions, other potential parameters were taken from the work of Moldauer [25]. However, it is well known that the valence model calculations scarcely depend on the optical potential, especially on the imaginary term of the central potential [26].

Table IV shows the calculated partial radiative widths of the 180-keV s-wave resonance in ^{28}Si. The neutron width was taken to be 31 keV. This value was redetermined from a Breit-Wigner multi-level fitting for neutron resonances in ^{28}Si [11], as it was found that the evaluated

TABLE VII. Partial radiative widths of the 658-keV s-wave resonance in ^{24}Mg.

		Partial radiative widths (eV)		
E_x (keV)	θ_f^2	Present	Valence	*CM*
585($\frac{1}{2}^+$)	0.51	0.59±0.42		(0.59)
975($\frac{3}{2}^+$)	0.35	0.45±0.15		(0.45)
2564($\frac{1}{2}^+$)	0.13			0.06
2801($\frac{3}{2}^+$)	0.36	0.23±0.13		0.19
3414($\frac{3}{2}^-$)	0.26	0.17±0.11	0.22	(0.17)
4277($\frac{1}{2}^-$)	0.19	−0.08±0.14	0.05	0.06
5474($\frac{1}{2}^+$)	0.17[a]	−0.11±0.13		0.01

[a]Reference [28].

neutron width, 60 keV, of Mughabghab *et al.* [10] is mistaken. The spectroscopic factors for low-lying states in ^{29}Si were taken from the evaluated values of Endt [27]. In the table, the observed partial radiative width for the 4934-keV ($\frac{3}{2}^-$) state transition is in substantial agreement with the calculated value. As for the 6381-keV ($\frac{1}{2}^-$) state transition, the calculated value is much smaller than the observed one. As mentioned in Sec. III A 1, this is because the observed width includes a large contribution of the cascade transition between the ground (0^+) and 2236-keV (2^+) states in ^{30}Si.

Table V shows the calculated partial widths of the 103-keV *s*-wave resonance in ^{32}S. For the neutron width, the evaluated value, 15 keV, of Mughabghab *et al.* [10] was used, and the spectroscopic factors were taken from the work of Endt [27] and Mermaz *et al.* [28]. A good agreement between the calculated and measured values is found for the 3220-keV ($\frac{3}{2}^-$) and 5715-keV ($\frac{1}{2}^-$) state transitions. However, the calculated value for the 4210-keV ($\frac{3}{2}^-$) state transition is much smaller than the observed one. As mentioned in Sec. III A 2, the reason is that the primary transition to this state is not distinguished from the primary $M1$ transitions to the 4055-keV ($\frac{1}{2}^+$) and 4425-keV ($\frac{1}{2}^+$) states.

Table VII shows the calculated partial widths of the 658-keV *s*-wave resonance in ^{24}Mg. The neutron width, 21 keV, was taken from an evaluation of Mughabghab *et al.* [10] and the spectroscopic factors from the work of Endt [27]. Then, it is found that the calculations reproduce the observed radiative widths for the 3414-keV ($\frac{3}{2}^-$) and 4277-keV ($\frac{1}{2}^-$) state transitions within the error.

Moreover, we show in Figs. 10(a) and 10(b) the wave function for the 658-keV *s*-wave resonance in ^{24}Mg and the radial part of the transition matrix element for valence-neutron capture to the 3414-keV ($\frac{3}{2}^-$) state in ^{25}Mg. As seen from the figures, a great success of the valence-capture model would be due to an extensive tail of the *s*-wave neutron resonance wave function and to a strong cancellation of the $E1$ transition matrix element in the nuclear internal region, resulting in a decoupling between the *s*-wave neutron single-particle transition and the giant dipole resonance (GDR) excitation in the target nucleus [29].

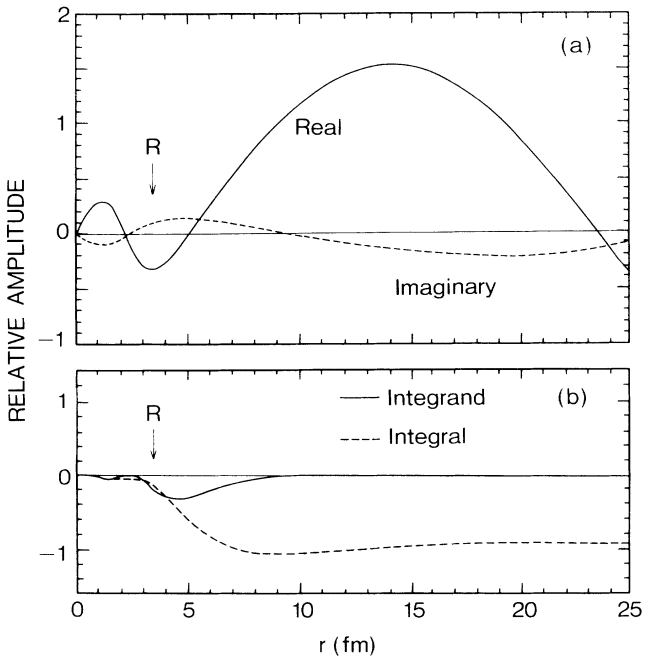

FIG. 10. (a) Wave function for the 658-keV *s*-wave resonance in ^{24}Mg. (b) Radial part of the transition matrix element for valence-neutron capture to the 3414-keV ($\frac{3}{2}^-$) state in ^{25}Mg.

B. Magnetic dipole transitions

In electromagnetic transitions from the broad *s*-wave neutron resonances in the *sd*-shell nuclei, ^{24}Mg, ^{28}Si, and ^{32}S, enhanced $M1$ transitions to low-lying states with a strong single-particle character have been observed, which make a sharp contrast with those from broad *p*-wave neutron resonances. The enhancement could be closely related to a core excitation of isovector 1^+ states which is aroused by coherent spin-flip transitions of filled $1d_{5/2}$-shell nucleons into the vacant $1d_{3/2}$-shell orbit. The excitation of isoscalar 1^+ states would be strongly suppressed in electromagnetic transitions. Thus, it is easily supposed from a weak-coupling model that the core-excitation configurations, $(1^+\otimes s_{1/2})$ and $(1^+\otimes d_{3/2})$, produced by coupling between isovector 1^+ states in the target nucleus and a *sd*-shell nucleon, are mixed into those resonance states.

On this viewpoint, we assume a configuration-mixing wave function for each resonance with the mixing amplitudes a, b, and c:

$$\Psi_i(\tfrac{1}{2}^+)=a(0^+\otimes s_{1/2})+b(1^+\otimes s_{1/2})+c(1^+\otimes d_{3/2}) , \tag{10}$$

where a, b, and c are determined from observed radiative widths. And the wave functions for low-lying states with $J^\pi(=\frac{1}{2}^+,\frac{3}{2}^+,\frac{1}{2}^-,\frac{3}{2}^-)$ are taken as

$$\Psi_f(\tfrac{1}{2}^+)=a_1(0^+\otimes s_{1/2})+\cdots , \tag{11}$$

$$\Psi_f(\tfrac{3}{2}^+)=a_2(0^+\otimes d_{3/2})+\cdots , \tag{12}$$

$$\Psi_f(\tfrac{1}{2}^-)=a_3(0^+\otimes p_{1/2})+\cdots , \tag{13}$$

and

$$\Psi_f(\tfrac{3}{2}^-)=a_4(0^+\otimes p_{3/2})+\cdots , \tag{14}$$

where a_i^2 is the spectroscopic factor of a final bound state, which is obtained from neutron-transfer reactions. Then, the partial radiative widths for primary $M1$ transitions to those states with $J^\pi(=\frac{1}{2}^+,\frac{3}{2}^+)$ are written as

$$\Gamma_{\gamma f}(\tfrac{1}{2}^+)=\frac{16}{9}\pi k_\gamma^3\frac{|(\Psi_f\|m^1\|\Psi_i(J))|^2}{2J+1} \tag{15}$$

$$=\tfrac{16}{9}\pi k_\gamma^3 a_1^2 b^2 B_\downarrow(M1) \tag{16}$$

and

$$\Gamma_{\gamma f}(\tfrac{3}{2}^+)=\tfrac{16}{9}\pi k_\gamma^3 a_2^2 c^2 B_\downarrow(M1) , \tag{17}$$

where $m_{1\mu}$ is the isovector magnetic-dipole operator on the *sd*-space of core-nucleus coordinates, and $B_{\downarrow}(M1)$ is the reduced isovector $M1$ strength of the core nucleus in the resonance state. Moreover, the mixing amplitudes, a, b, and c, satisfy the relation

$$a^2+b^2+c^2=1.0\ . \tag{18}$$

In Sec. IV A, it was shown that the primary $E1$ transitions are successfully explained by the valence-capture model. Therefore, the partial radiative widths for the primary $E1$ transitions to those states with $J^{\pi}(=\frac{1}{2}^-,\frac{3}{2}^-)$ may be described as

$$\Gamma_{\gamma f}(\tfrac{1}{2}^-)=\tfrac{16}{9}\pi k_{\gamma}^3 a_3^2 a^2 B_{\downarrow}(E1) \tag{19}$$

and

$$\Gamma_{\gamma f}(\tfrac{3}{2}^-)=\frac{16}{9}\pi k_{\gamma}^3 a_4^2 a^2 B_{\downarrow}(E1)\ , \tag{20}$$

where the reduced $E1$ strength, $B_{\downarrow}(E1)$, is taken to be the Weisskopf unit (W.u.) of 8.63×10^5 eV fm^3.

Using Eqs. (16)–(20) and the observed widths in parentheses in Tables IV, V, and VII, the mixing amplitudes are determined, except for the phase factor:

$$\Psi_i(^{29}\mathrm{Si})=\sqrt{0.047}(0^+\otimes s_{1/2})+\sqrt{0.519}(1^+\otimes s_{1/2}) +\sqrt{0.434}(1^+\otimes d_{3/2})\ , \tag{21}$$

$$\Psi_i(^{33}\mathrm{S})=\sqrt{0.027}(0^+\otimes s_{1/2})+\sqrt{0.696}(1^+\otimes s_{1/2}) +\sqrt{0.277}(1^+\otimes d_{3/2})\ , \tag{22}$$

and

$$\Psi_i(^{25}\mathrm{Mg})=\sqrt{0.011}(0^+\otimes s_{1/2})+\sqrt{0.428}(1^+\otimes s_{1/2}) +\sqrt{0.561}(1^+\otimes d_{3/2})\ . \tag{23}$$

The $B_{\downarrow}(M1)$ values are obtained to be $0.708\mu_n^2$ for ^{28}Si, $0.651\mu_n^2$ for ^{32}S, and $0.572\mu_n^2$ for ^{24}Mg with the square of a nuclear magneton, μ_n^2. Those quantities are connected to the reduced $M1$ strengths, $B_{\uparrow}(M1)$:

$$B_{\uparrow}(M1;I_1\rightarrow I_2)=\frac{2I_2+1}{2I_1+1}B_{\downarrow}(M1;I_2\rightarrow I_1)\ , \tag{24}$$

where I_1 and I_2 are the spins of the ground and excited states in the core nucleus, respectively. As a consequence, we find that the $B_{\uparrow}(M1)$ values are $2.124\mu_n^2$ for ^{28}Si, $1.953\mu_n^2$ for ^{32}S, and $1.716\mu_n^2$ for ^{24}Mg. The values seem to be consistent with the summed reduced isovector $M1$ strengths, $B_{\uparrow}(M1)$, below the excitation energy of 11 MeV [30], obtained using (p,p'), (γ,γ'), and (e,e') reactions on ^{24}Mg, ^{28}Si, and ^{32}S.

From the above wave functions, we can derive the partial radiative widths [configuration mixing (CM)] for primary $E1$ and $M1$ transitions to all the final states, as shown in Tables IV, V, and VII. The partial radiative widths in parentheses were used to determine the mixing amplitudes for the wave function of each resonance state. As seen from the tables, the electric and magnetic dipole transitions from those s-wave resonances would be reasonably understood by the configuration-mixing wave function given in Eq. (10).

Here, it is worthwhile to mention large-scale shell-model calculations with a universal effective interaction. For the even-even *sd*-shell nuclei, ^{24}Mg, ^{26}Mg, ^{28}Si, and ^{32}S, the experimentally deduced B (σ) values by inelastic proton scattering were compared with theoretical calculations and other experimental B($M1$) values obtained from (e,e') and (γ,γ') reactions [30]. Consequently, it was found that the wave functions in the model space of a

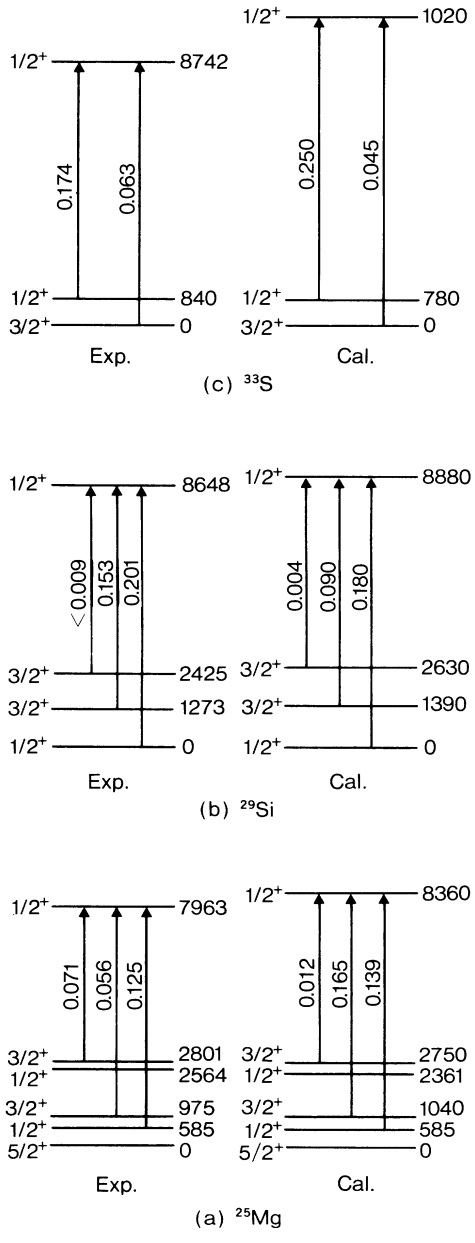

FIG. 11. Observed and calculated strengths for s-wave neutron resonance $M1$ transitions. The strengths are shown in units of the square of a nuclear magneton, μ_n^2. The experimentally deduced $B_{\downarrow}(M1)$ values are transformed to the $B_{\uparrow}(M1)$ values on the final states. The calculated energy levels and $B_{\uparrow}(M1)$ values are obtained by the full-space *sd*-shell model with the effective interaction of Wildenthal [31].

full $(sd)^n$ configurations with the effective interation of Wildenthal [31] are able to reproduce the observed excitation energies of 1^+ states and the observed reduced matrix elements of $M1$ transitions from the ground states in those nuclei.

In the present study, we also try to calculate $B_\uparrow(M1)$ values, using the large-scale shell model with the universal effective interaction in the *sd* shell, and to compare those values with the observed $B_\uparrow(M1)$ values in the odd A nuclei deduced from *s*-wave neutron resonance capture by the even-even target nuclei. The results for ^{25}Mg, ^{29}Si, and ^{33}S are shown in Figs. 11(a)–(c). Only the relevant levels and $B_\uparrow(M1)$ values are presented in the figures. One can easily see that the model reproduces the observed $M1$ transitions fairly well with no specific assumption. The reduced matrix elements for $M1$ transition are then evaluated with the free-nucleon g factor.

V. SUMMARY

We have observed electromagnetic transitions from the broad *s*-wave neutron resonances at 658 keV in ^{24}Mg, at 180 keV in ^{28}Si, and at 103 keV in ^{32}S. As a result, enhanced $E1$ and $M1$ transitions were found to low-lying states with a strong single-particle character. The $E1$ transitions are well explained by the valence-capture model. The great success of this model would be due to the fact that the valence-transition matrix elements cancel out in the nuclear internal region, and therefore those transitions decouple from GDR. Moreover, we conclude that the enhancement of $M1$ transitions would result from the excitation of isovector $M1$ states in the core nucleus.

[1] B. J. Allen, A. R. de L. Musgrove, R. L. Macklin, and R. R. Winters, in *Proceedings of a Specialist's Meeting on Neutron Data of Structural Materials for Fast Reactors,* Geel, Belgium, 1977, edited by K. H. Böckhoff (Pergamon, New York, 1978), p. 506.

[2] M. Shimizu, M. Igashira, K. Terazu, and H. Kitazawa, Nucl. Phys. **A452**, 205 (1986).

[3] T. Uchiyama, M. Igashira, and H. Kitazawa, Phys. Rev. C **41**, 862 (1990).

[4] H. Kitazawa, M. Igashira, Y. Achiha, N. Mukai, F. Uesawa, T. Andoh, and S. Shibata, Nucl. Phys. **A536**, 109 (1992).

[5] C. M. McCullagh, M. L. Stelts, and R. E. Chrien, Brookhaven National Laboratory Report No. BNL-28515 (1980).

[6] A. Bohr and B. R. Mottelson, *Nuclear Structure* (Benjamin, Mass., 1975), Vol. II, p. 638.

[7] M. Igashira, H. Kitazawa, and N. Yamamuro, Nucl. Instrum. Methods **A245**, 432 (1986).

[8] M. Shimizu, Ph.D. thesis, Tokyo Institute of Technology, 1985.

[9] M. Igashira, H. Kitazawa, M. Shimizu, H. Komano, and N. Yamamuro, Nucl. Phys. **A457**, 301 (1986).

[10] S. F. Mughabghab, M. Divadeenam, and N. E. Holden, *Neutron Cross Sections* (Academic, New York, 1981), Vol. 1.

[11] H. Kitazawa, Y. Harima, and T. Fukahori, in *Proceedings of the International Conference on Nuclear Data for Science and Technology,* Mito, 1988, edited by S. Igarasi (Saikon, Tokyo, 1988), p. 473.

[12] ENDF/B-V data file for ^{197}Au (MAT=1379), evaluated by S. F. Mughabghab (1979).

[13] R. L. Macklin and J. H. Gibbons, Phys. Rev. **159**, 1007 (1967).

[14] L. Harris, Jr., H. Kendrik, and S. M. Sperling, An Introduction to the Principles and Use of the FERDOR Unfolding Code, offered by Gulf Radiation Technology, California (1970).

[15] H. Kitazawa, M. Ohgo, T. Uchiyama, and M. Igashira, Nucl. Phys. **A464**, 61 (1987).

[16] M. M. Aleonard, D. Castera, P. Hubert, F. Leccia, P. Mennrath, and J. P. Thibaud, Nucl. Phys. **A146**, 90 (1970).

[17] J. R. Bird, B. J. Allen, I. Berggvist, and J. A. Biggerstaff, Nucl. Data Tables **11**, 433 (1973).

[18] P. M. Endt and C. Van der Leun, Nucl. Phys. **A310**, 1 (1978).

[19] S. Raman, R. F. Carlton, J. C. Wells, E. T. Jurney, and J. E. Lynn, Phys. Rev. C **32**, 18 (1985).

[20] A. M. Lane and J. E. Lynn, Nucl. Phys. **17**, 563 (1960).

[21] H. Kitazawa, Triangle Universities Nuclear Laboratory Annual Report TUNL-XIX (1980), p. 114.

[22] H. Kitazawa and M. Igashira, J. Phys. **G14**, S215 (1988).

[23] H. Kitazawa and K. Hida, unpublished.

[24] A. M. Lane and S. F. Mughabghab, Phys. Rev. C **10**, 412 (1974).

[25] P. A. Moldauer, Nucl. Phys. **47**, 65 (1963).

[26] R. F. Barrett and T. Terasawa, Nucl. Phys. **A240**, 445 (1975).

[27] P. M. Endt, At. Data Nucl. Data Tables **19**, 23 (1977).

[28] M. C. Mermaz, C. A. Whitten, Jr., J. W. Champlin, A. J. Howard, and D. A. Bromley, Phys. Rev. C **4**, 1778 (1971).

[29] A. Bohr and B. R. Mottelson, in *Proceedings of the International Symposium on Neutron Capture Gamma-Ray Spectroscopy,* Studsvik, Sweden, 1969 (IAEA, Vienna, 1969), p. 3.

[30] G. M. Crowley, C. Djalali, N. Marty, M. Morlet, A. Willis, N. Anantaraman, B. A. Brown, and A. Galonsky, Phys. Rev. C **39**, 311 (1989).

[31] B. H. Wildenthal, in *Progress in Particle and Nuclear Physics,* edited by D. H. Wilkinson (Pergamon, Oxford, 1984), Vol. 11, p. 5.